

---

# Coarsening Linear Non-Gaussian Causal Models with Cycles

---

**Francisco Madaleno**

Department of Technology, Management and Economics,  
 Technical University of Denmark  
 fmfsa@dtu.dk

**Francisco C Pereira**

Department of Technology, Management and Economics,  
 Technical University of Denmark

**Alex Markham**

Department of Mathematical Sciences,  
 University of Copenhagen

## Abstract

Recent work on causal abstraction, in particular graphical approaches focusing on causal structure between clusters of variables, aims to summarize a high-dimensional causal structure in terms of a low-dimensional one. Existing methods for learning such summaries from data assume that both the high- and low-dimensional structures are acyclic, which is helpful for causal effect identification and reasoning but excludes many high-dimensional models and thus limits applicability. We show that in the linear non-Gaussian (LiNG) setting, the high-dimensional acyclicity assumption can be relaxed while still allowing recovery of a low-dimensional causal directed acyclic graph (DAG). We further connect identifiability of this low-dimensional DAG to existing results: LiNG models with cycles are observationally identifiable only up to an equivalence class whose members differ by reversals of directed cycles; our low-dimensional DAG, which is invariant across all members of a given equivalence class, thus forms a natural representative of the class. While existing approaches for learning this observational equivalence class over high-dimensional variables have exponential time complexity, our low-dimensional summary is learned in worst-case cubic time and comes with explicit bounds on the sample complexity. We provide open source code and experiments on synthetic data to corroborate our theoretical results.

## 1 Introduction

Causal discovery from observational data has predominantly focused on directed *acyclic* graphs (DAGs) [32, 33]. Yet many systems of scientific interest contain feedback loops: gene-regulatory networks [29] and dynamical systems [24] exhibit directed cycles. A line of work on *cyclic* causal models has therefore developed, ranging from the structural-equation formulation of [34, 5] to the linear non-Gaussian models of [19], which exploit standard ICA [16, 11] to recover the demixing matrix  $W = I - B$  of a linear cyclic Structural Causal Model (SCM) up to row permutation and scaling, from which the weighted adjacency matrix  $B$ —and hence the directed graph  $G$ —can be recovered up to a distributional equivalence class. Additionally, other approaches have tried to identify causal orderings among groups of variables: early extensions of linear non-Gaussian methods

introduced techniques to estimate causal orderings among multidimensional, disjoint sets of variables [17, 10]. The GroupLiNGAM algorithm of [17] has worst-case complexity exponential in the number of variables. More recently, this perspective has been revisited for models containing disjoint cycles [9], with identification results that rely on second- and third-order moments and thus require the noise distribution to be skewed. In contrast, our approach relies only on general non-Gaussianity via standard ICA, does not require disjoint cycles, and runs in polynomial time. We provide an empirical comparison with that line of work, even though their identification target (the full variable-level cyclic graph under disjoint cycles) differs from ours.

The coarsening framework of [38, 21] characterizes when a DAG can be simplified by grouping variables into clusters. We show that this framework extends naturally to directed graphs with cycles: the strongly connected components (SCC) partition emerges as a structural floor on the coarsening lattice—the finest partition whose quotient is a DAG—and the resulting cluster-DAG is exactly the *condensation*  $G^{\text{sc}}$  of  $G$  in the classical sense of graph theory [4]. This is the identification target that resolves the ambiguity in the equivalence class of [19].

**Contributions.** We extend the coarsening framework to directed graphs that may contain cycles, and connect it to the cyclic-SCM identification literature:

- **The SCC floor (§ 4.1).** The coarsening lattice acquires a structural floor: any valid DAG-coarsening must group nodes in a common SCC, and the SCC partition is the finest valid one.
- **Condensation identifiability (Theorem 1, § 4.2).** The condensation  $G^{\text{sc}}$  of a linear non-Gaussian cyclic SCM is invariant across the distributional equivalence class of [19], and is therefore identifiable from observational data alone, without invoking the stability and disjoint-cycles assumptions of that work.

As a downstream payoff, identifying  $G^{\text{sc}}$  from observations alone supplies the prerequisite of the C-DAG identification theorems of [2], reducing cluster-level causal-effect identification in a cyclic system to the standard acyclic case.

The paper is organized as follows: § 3 fixes notation and recalls the coarsening lattice and cyclic-SCM background; § 4 introduces DAG-coarsenings of cyclic graphs, proves the SCC-floor proposition, presents the learning procedure, proves condensation identifiability and discusses the implication for cluster-level causal-effect identification; § 5 reports the synthetic experiments<sup>1</sup>; § 6 concludes.

## 2 Related Work

**Cyclic generalisations of structural causal models** date back to [34], with rigorous foundations in [5]. [19] showed that linear non-Gaussian cyclic SCMs with no latent confounders can be identified via standard ICA: ICA recovers the demixing matrix  $\hat{W}$ , from which one obtains a candidate adjacency matrix  $\hat{B} = I - \text{diag}(P\hat{W})^{-1}P\hat{W}$  for each admissible row permutation  $P$ , and thresholding yields the graph. Later work has extended this to latent-confounded settings via overcomplete ICA [30, 7], extensions of LiNGAM [22], and constraint-based methods using  $\sigma$ -separation [12]. [1] study structure learning for linear cyclic SCMs including the Gaussian case, while [36] adapt linear non-Gaussian models to learn graphs that are polytrees and [27] leverages interventional data. The condensation also appears in recent experiment-design work for linear non-Gaussian cyclic models [31]; our contribution is to place this invariance inside the coarsening lattice as its structural floor, connecting it to the broader coarsening/abstraction literature and to C-DAG identification.

Another line of work grounds causal models in **stochastic differential equations** [13], rather than standard structural equations. Graphical Lyapunov models [37, 8, 25, 26] encode directed causal structure via a weighted adjacency matrix that solves either the continuous- and discrete-time Lyapunov equation, while naturally allowing for cycles.

**Coarsening of causal models** has been approached from several angles: causal abstraction in the SCM sense [28, 3], group-level structure under partial-order assumptions [38] and the partition-refinement approach of [21] that we extend here. The C-DAG identification theorems of [2] characterize which cluster-level interventional distributions are recoverable once an acyclic cluster-level

<sup>1</sup>An open source implementation as well as scripts for reproducing all of the following experiments can be found at <https://github.com/fmfsa/coarsening-cycles>.

graph is given; the condensation we identify in this paper is precisely such a graph, supplied from observational data.

The condensation construction is standard in **graph theory**; [35] gives a linear-time algorithm. Our use of the SCC partition as the finest valid DAG-coarsening is, to our knowledge, new in the causal-discovery context: it transforms a cyclic model into an acyclic surrogate to which the standard causal effect identification machinery for DAGs applies.

### 3 Background

#### 3.1 Coarsening causal models

Let  $G^* = (V^*, E^*)$  be a DAG. A *coarsening* [21] of  $G^*$  is a partition  $\Pi = \{\pi_1, \dots, \pi_k\}$  of  $V^*$  such that the quotient graph  $G' = (\Pi, E')$  with edges

$$E' = \{(\chi(u^*), \chi(v^*)) \mid (u^*, v^*) \in E^*, \chi(u^*) \neq \chi(v^*)\}$$

is itself a DAG, where  $\chi : V^* \rightarrow \Pi$  sends each node to its part. We call  $G'$  the *quotient graph* and the parts  $\pi_i$  *clusters*.

The set of all coarsenings of  $G^*$  ordered by refinement forms a sublattice of the partition refinement lattice (Theorem 3 in [21]); we generalize this construction to cyclic graphs in § 4.

#### 3.2 Cyclic structural causal models

A linear cyclic SCM is defined by:

$$X = BX + \varepsilon, \quad \text{solved as } X = (I - B)^{-1}\varepsilon, \quad (1)$$

where  $d = |V|$  is the number of variables,  $B \in \mathbb{R}^{d \times d}$  is the weighted adjacency matrix of a directed graph  $G = (V, E)$  (which may contain cycles), and the noise vector  $\varepsilon \in \mathbb{R}^d$  has mutually independent components. The spectral radius  $\rho(B) = \max_i |\lambda_i(B)|$  controls when (1) is solvable: existence and uniqueness require only  $\det(I - B) \neq 0$ , while the stronger condition  $\rho(B) < 1$  additionally ensures dynamical stability of the underlying iteration and is the regime studied by [19].

Two matrices play distinct roles. The *mixing matrix*  $A = (I - B)^{-1}$  maps independent sources to observations,  $X = A\varepsilon$ ; its support encodes the transitive closure of  $G$  (i.e., total effects/reachability) under no exact cancellations. The *demixing matrix*  $W = I - B = A^{-1}$  recovers sources from observations via  $\varepsilon = WX$ ; its off-diagonal support encodes the *direct* adjacency of  $G$ . Throughout,  $\widehat{W}$  denotes the sample-level FastICA estimate of  $W$ .

### 4 Coarsening Directed Graphs with Cycles

We first generalize the notion of coarsening from DAGs to directed graphs that may contain cycles.

**Definition 1** (DAG-coarsening of a directed graph). *Let  $G = (V, E)$  be a directed graph (possibly containing cycles), and let  $\Pi = \{\pi_1, \dots, \pi_k\}$  be a partition of  $V$  with associated surjection  $\chi : V \rightarrow \Pi$ . The quotient graph is  $G' = (\Pi, E')$  with*

$$E' = \{(\chi(u), \chi(v)) \mid (u, v) \in E, \chi(u) \neq \chi(v)\}.$$

*We call  $\Pi$  a DAG-coarsening of  $G$  when  $G'$  is acyclic.*

When  $G$  is a DAG this reduces to the original definition of [21]: the trivial singleton-per-node partition has an acyclic quotient, and so does any coarsening of it. For graphs containing cycles the acyclicity requirement is non-trivial and forces SCCs to be respected, as Proposition 1 below shows.

#### 4.1 The SCC floor

**Definition 2** (SCC coarsening/condensation). *Given a directed graph  $G = (V, E)$ , the SCC coarsening of  $G$  is the DAG-coarsening whose partition surjection  $\chi$  satisfies*

$$\text{for all } v, w \in V, \quad \chi(v) = \chi(w) \iff \text{sc}_G(v) = \text{sc}_G(w),$$

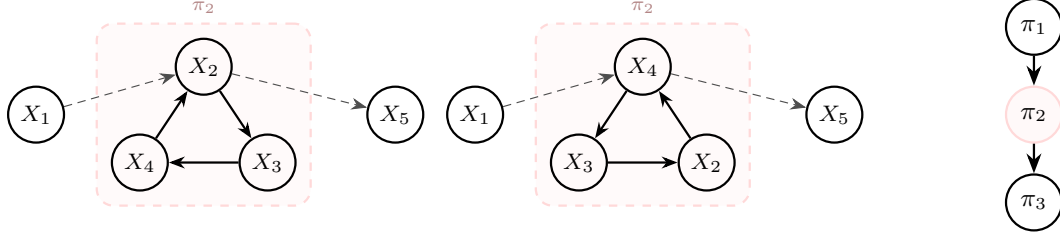


Figure 1: Distributional equivalence and condensation for the five-variable cyclic SCM of [19] (Example 1). (left, center) Two members of the distributional equivalence class recovered by ICA, differing only in the orientation of the 3-cycle inside the SCC  $\pi_2 = \{X_2, X_3, X_4\}$ ; both correspond to admissible permutations of the demixing matrix  $\widehat{W}$ . (right) The shared condensation  $G^{\text{sc}}$  with clusters  $\pi_1 = \{X_1\}$ ,  $\pi_2 = \{X_2, X_3, X_4\}$ ,  $\pi_3 = \{X_5\}$ . ICA cannot distinguish (left) from (center), but  $G^{\text{sc}}$  is identifiable (Theorem 1). Note that the inter-SCC edge from  $X_1$  lands on  $X_2$  in (left) and on  $X_4$  in (center); the cluster-level edge  $\pi_1 \rightarrow \pi_2$  of  $G^{\text{sc}}$  is unchanged.

where  $\text{sc}_G(v)$  is the strongly connected component of  $G$  containing  $v$ . The induced quotient is the condensation of  $G$  [4], denoted  $G^{\text{sc}}$ . The underlying partition coincides with the maximally acyclic partition of [38] (their Definition 8(ii)).

**Proposition 1** (SCC floor). *Let  $G = (V, E)$  be a directed graph. Nodes  $u, v \in V$  in the same SCC of  $G$  must lie in the same cluster of every DAG-coarsening of  $G$ . Consequently, the SCC coarsening of Definition 2 is the finest DAG-coarsening of  $G$ , and its quotient  $G^{\text{sc}}$  is the structural floor of the DAG-coarsening sublattice.*

*Proof.* If  $u$  and  $v$  are in the same SCC, there exist directed paths  $u \rightarrow \dots \rightarrow v$  and  $v \rightarrow \dots \rightarrow u$  in  $G$ . If  $\chi(u) \neq \chi(v)$  in a coarsening, these paths induce directed paths  $\chi(u) \rightarrow \dots \rightarrow \chi(v)$  and  $\chi(v) \rightarrow \dots \rightarrow \chi(u)$  in the quotient, forming a cycle and violating the DAG requirement.  $\square$

Given  $G$  the SCC partition is computable via Tarjan’s algorithm [35].

**Remark 1** (cyclic coarsenings). *Definitions 1 and 2 requires the coarsened graph to be a DAG, mirroring the original framework of [21]. A natural generalization drops this requirement and asks only that the coarsening preserves the partial order over SCCs of  $G$ : any partition  $\chi$  such that the quotient graph (a) does not reverse a non-cyclic ancestral relation in  $G$ , and (b) does not introduce a cycle between nodes that are not already in a common SCC, is a valid cyclic coarsening. The interventional and observational coarsenings considered below are all DAG-coarsenings (and hence cyclic coarsenings), so we focus on the DAG case throughout. Characterizing the general cyclic-coarsening lattice is left to future work.*

**Example 1** (example of [19]). *Consider the five-variable linear cyclic SCM*

$$X_1 = \varepsilon_1, \quad X_2 = 1.2 X_1 - 0.3 X_4 + \varepsilon_2, \quad X_3 = 2 X_2 + \varepsilon_3, \quad X_4 = -X_3 + \varepsilon_4, \quad X_5 = 3 X_2 + \varepsilon_5.$$

*The directed graph has edges  $X_1 \rightarrow X_2$ ,  $X_2 \rightarrow X_3$ ,  $X_3 \rightarrow X_4$ ,  $X_4 \rightarrow X_2$  (a 3-cycle), and  $X_2 \rightarrow X_5$  (Figure 1 left). The cycle  $X_2 \rightarrow X_3 \rightarrow X_4 \rightarrow X_2$  forms the unique non-trivial SCC  $\{X_2, X_3, X_4\}$ ; nodes  $X_1$  and  $X_5$  are singletons. Since any DAG-coarsening must absorb each SCC into a single cluster (Proposition 1), the finest valid coarsening has three clusters  $\pi_1 = \{X_1\}$ ,  $\pi_2 = \{X_2, X_3, X_4\}$ ,  $\pi_3 = \{X_5\}$ , yielding the chain condensation  $G^{\text{sc}} = \pi_1 \rightarrow \pi_2 \rightarrow \pi_3$  in Figure 1, right. Reversing the 3-cycle to  $X_2 \rightarrow X_4 \rightarrow X_3 \rightarrow X_2$  (Figure 1, center) yields a second variable-level graph with re-weighted edges that induces the same observational distribution [19, Theorem 4]: ICA cannot distinguish the two, but they share the condensation  $G^{\text{sc}}$ —the invariance that Theorem 1 formalizes.*

**Remark 2** (combinatorial structure). *For  $n = 5$  the partition lattice has  $B_5 = \sum_{k=1}^5 S(5, k) = 1 + 15 + 25 + 10 + 1 = 52$  partitions, where  $S(n, k)$  is the Stirling number of the second kind. Only 4 are valid DAG-coarsenings of Example 1: the singleton, the SCC floor  $\{X_1\} \mid \{X_2, X_3, X_4\} \mid \{X_5\}$ , and the two intermediate 2-clusters  $\{X_1\} \mid \{X_2, X_3, X_4, X_5\}$  and  $\{X_1, X_2, X_3, X_4\} \mid \{X_5\}$ . The remaining 48 are invalid for two reasons (Figure 2): they either split the SCC  $\{X_2, X_3, X_4\}$ , or they merge across condensation layers (e.g.  $\{X_1, X_5\} \mid \{X_2, X_3, X_4\}$ , where the edges  $X_1 \rightarrow X_2$  and  $X_2 \rightarrow X_5$  create a cycle in the quotient).*

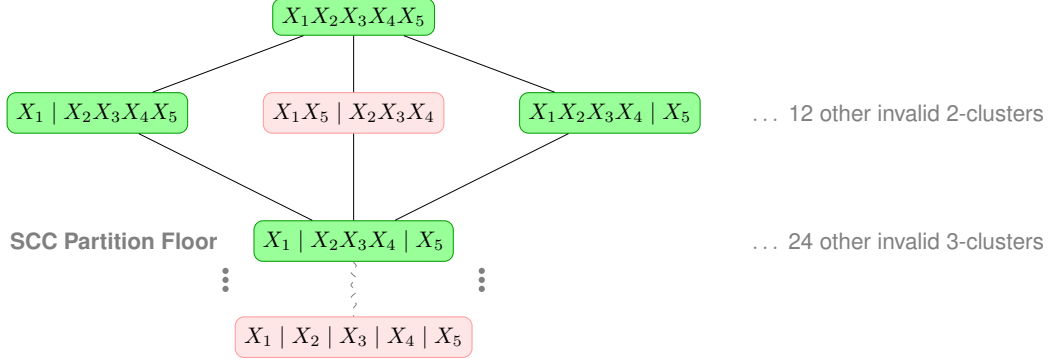


Figure 2: The valid DAG-coarsening sublattice (green) for the graph of [Example 1](#), embedded in the full partition lattice ( $B_5 = 52$  partitions). Only 4 of the 52 partitions are valid. The 2-cluster node  $\{X_1, X_5\} | \{X_2, X_3, X_4\}$  is invalid not because it splits an SCC but because merging  $X_1$  and  $X_5$  creates a cycle between the two clusters. All partitions below the SCC floor split  $\{X_2, X_3, X_4\}$  and are likewise invalid.

## 4.2 Observational coarsening via linear non-Gaussian ICA

We assume the linear cyclic SCM of (1) with mutually independent, non-Gaussian noise components  $\varepsilon_i$  and *no latent confounders*, so  $\varepsilon$  has the same dimension as  $X$ . Under these assumptions, standard ICA [11] recovers  $W = I - B$  up to row permutation and scaling—the regime exploited by [19]. Overcomplete ICA [20] is needed only when the number of independent sources exceeds the number of observed variables, which arises under latent confounding [30, 7]. The interventional case is discussed in [Appendix A.1](#).

Let  $\hat{W}$  denote the ICA estimate. Each row permutation  $P$  such that  $P\hat{W}$  has nonzero diagonal entries yields an admissible candidate:

$$\hat{B}_P = I - \text{diag}(P\hat{W})^{-1} P\hat{W}. \quad (2)$$

The off-diagonal support of  $\hat{B}_P$ , after thresholding at  $\tau$ , gives a candidate directed graph  $\hat{G}_P$ . Different admissible permutations  $P$  yield different members of the distributional equivalence class. [19] resolve this ambiguity by selecting the first candidate with  $\rho(\hat{B}_P) < 1$ , the *first-stable filter*, which under their stability assumption recovers the true  $B$ .

**Theorem 1** (Condensation identifiability). *Let  $G_1, G_2$  be two directed graphs underlying linear cyclic SCMs of the form (1), both with no latent confounders, mutually independent noise terms and at most one Gaussian noise component. If they induce the same observational distribution over  $X$ , then their condensations are equal:  $G_1^{\text{sc}} = G_2^{\text{sc}}$  (same SCC partition, same set of inter-SCC edges).*

*Proof.* By Theorem 4 of [19], equality of distributions implies  $G_2$  is obtained from  $G_1$  by a sequence of directed-cycle reversals.<sup>2</sup>

*SCC partition.* Each reversal acts only on edges that lie on a directed cycle and is therefore confined to a single SCC of  $G_1$ . Within that SCC, the reversal reassigns the structural equations of the nodes on the cycle but preserves mutual reachability: every node on the reversed cycle retains directed paths to and from every other node on it. Nodes outside the SCC are unaffected. Hence  $G_1$  and  $G_2$  have the same SCC partition.

*Inter-cluster edges of  $G^{\text{sc}}$ .* An inter-SCC edge  $u \rightarrow v$  of  $G$  lies on no directed cycle: any cycle through it would make  $u$  and  $v$  mutually reachable, hence in the same SCC. Cycle reversal acts only on edges that lie on directed cycles, so it cannot remove or add an inter-SCC edge. It can reassign the structural equation associated with a node *inside* an SCC, which shifts the variable-level endpoint of an incoming inter-SCC edge to a different node within the same SCC; the cluster-level edge of  $G^{\text{sc}}$  is unchanged. Combined with the SCC equality above, this gives  $G_1^{\text{sc}} = G_2^{\text{sc}}$ .  $\square$

<sup>2</sup>Characterizations in the latent-variable/overcomplete-ICA setting: [7].

---

**Algorithm 1** Condensation recovery from observational data.
 

---

**Require:** Observations  $X \in \mathbb{R}^{n \times d}$ , threshold  $\tau > 0$

**Ensure:** Condensation  $\widehat{G}^{\text{sc}} = (\widehat{\Pi}, \widehat{E}')$

- 1:  $\widehat{W} \leftarrow \text{FASTICA}(X, d)$  ▷ [15],  $d$  components
  - 2:  $P \leftarrow \text{HUNGARIAN}(\widehat{W})$  ▷ single admissible permutation;  $|(P\widehat{W})_{ii}| > \eta$  for tolerance  $\eta$
  - 3:  $\widehat{B} \leftarrow I - \text{diag}(P\widehat{W})^{-1} P\widehat{W}$  ▷ from (2)
  - 4:  $\widehat{B}_{ij} \leftarrow 0$  whenever  $|\widehat{B}_{ij}| < \tau$  ▷ thresholding
  - 5:  $\widehat{\Pi} \leftarrow \text{TARJAN}(\text{supp}(\widehat{B})^\top)$  ▷ SCCs [35]
  - 6:  $\widehat{E}' \leftarrow \{(\pi', \pi) : \pi \neq \pi', \exists (i, j) \in \text{supp}(\widehat{B}) \text{ with } i \in \pi, j \in \pi'\}$  ▷  $B_{ij} \neq 0$  encodes  
 $X_j \rightarrow X_i$
  - 7: **return**  $\widehat{G}^{\text{sc}} = (\widehat{\Pi}, \widehat{E}')$
- 

**Corollary 1.** *In the large-sample limit,  $G^{\text{sc}}$  is recoverable by running FastICA to obtain  $\widehat{W}$ , picking one admissible row permutation via the Hungarian algorithm [18] to obtain a candidate  $\widehat{B}$  via (2), and applying Tarjan’s algorithm to  $\text{supp}(\widehat{B})$ . Theorem 1 guarantees that the choice of admissible representative does not affect the recovered condensation.*

**Markov on the condensation.** A second consequence of SCC aggregation is the validity of conditional-independence reasoning at the cluster level.

**Lemma 1** (Markov on the condensation). *Under the linear cyclic SCM of (1), the marginal joint distribution on cluster-level features is Markov to the condensation  $G^{\text{sc}}$ .*

Linear cyclic SCMs are  $\sigma$ -Markov to  $G$  [34, 5]. Aggregating variables to their SCC clusters projects  $\sigma$ -separation statements about  $G$  onto separation statements about  $G^{\text{sc}}$ ; since  $G^{\text{sc}}$  is acyclic,  $\sigma$ -separation collapses to ordinary d-separation, so the cluster-level distribution is Markov to  $G^{\text{sc}}$ . Furthermore our identification does not invoke faithfulness: Algorithm 1 recovers  $\widehat{G}^{\text{sc}}$  by thresholding entries of  $\widehat{B}$ , not by conditional-independence testing, so faithfulness plays no role in Theorem 1. Nonetheless, Corollary 2 of [38] shows it transfers cleanly under the SCC partition:  $\sigma$ -Markovian and  $\sigma$ -faithful  $G$  implies the same for  $G^{\text{sc}}$ .

Algorithm 1 packages this as a procedure requiring only observational data, based on ICA-LiNG-D [19] composed with Tarjan, viewed through the coarsening lattice. Bounds on the sample complexity, in terms of  $\beta_{\min}$  the minimum nonzero entry of  $B$ , are provided in Appendix B.3. In particular, recovering the data-generating  $G^{\text{sc}}$  with probability at least  $1 - \delta$  requires sample size  $n = \Theta\left(\frac{d}{\beta_{\min}^2 \sqrt{\delta}}\right)$ .

Enumerating all admissible permutations (the original recipe of [19]) is unnecessary for our identification target: by Theorem 1,  $\widehat{G}^{\text{sc}}$  does not depend on the choice of admissible permutation, and Corollary 1 gives consistency of Algorithm 1 in the large-sample limit.

**Proposition 2** (Two failure modes of thresholding). *Finite-sample noise affects the recovered partition in two opposite directions. (a) A true intra-SCC edge whose magnitude falls below  $\tau$  is dropped; if this breaks reachability inside an SCC, the estimated partition splits a true SCC into multiple clusters. (b) A spurious entry surviving above  $\tau$  adds a false edge; if it closes a directed path between two distinct SCCs, the estimated partition merges them. Mode (b) yields a coarsening of the true SCC partition; mode (a) yields a refinement and the resulting quotient is, in general, not a valid DAG-coarsening of the true graph.*

We probe both failure modes empirically in Appendix C.2 and discuss their connection to the sample complexity in Appendix B.3.

**Theorem 2** (Time Complexity). *Let  $d = |V|$  be the number of observed variables and  $n$  the sample size. Algorithm 1 recovers  $G^{\text{sc}}$  in worst-case time  $\mathcal{O}(k \cdot n \cdot d^2 + d^3)$ , where  $k$  denotes the number of FastICA iterations to convergence.*

The proof and a step-by-step breakdown are in Appendix B.1. Because reliable ICA estimation requires  $n \gg d$ , the  $\mathcal{O}(k \cdot n \cdot d^2)$  term dominates in practice. By targeting  $G^{\text{sc}}$  rather than enumerating the full distributional equivalence class, we avoid the worst-case  $\mathcal{O}(d!)$  N-rooks bottleneck.

### 4.3 Causal Effect Identification on the Condensation

**Interventions in cyclic SCMs.** Under a soft (shift) intervention  $X^I = (I - B)^{-1}(\varepsilon + \delta)$ , effects propagate through the entire graph, including back through cycles. Hard (do) interventions that set a single variable  $X_k = c$  are excluded: they sever the equation for  $X_k$ , breaking the cyclic mechanism and potentially rendering the system inconsistent. However, hard interventions that target every node of a cluster  $\pi$  respect the SCC structure and yield well-defined interventional distributions on  $G^{\text{sc}}$ , which we describe next.

Fix a cluster  $\pi \subseteq V$  and let  $\bar{\pi} = V \setminus \pi$ . Partition  $X$ ,  $\varepsilon$ , and  $B$  accordingly:

$$X = \begin{pmatrix} X_\pi \\ X_{\bar{\pi}} \end{pmatrix}, \quad \varepsilon = \begin{pmatrix} \varepsilon_\pi \\ \varepsilon_{\bar{\pi}} \end{pmatrix}, \quad B = \begin{pmatrix} B_{\pi\pi} & B_{\pi\bar{\pi}} \\ B_{\bar{\pi}\pi} & B_{\bar{\pi}\bar{\pi}} \end{pmatrix}.$$

A *hard cluster intervention*  $\text{do}(X_\pi = c)$  replaces the equations indexed by  $\pi$  with  $X_\pi = c$ . Solving the remaining  $|\bar{\pi}|$ -system gives  $X_{\bar{\pi}} = (I - B_{\bar{\pi}\bar{\pi}})^{-1}(B_{\bar{\pi}\pi}c + \varepsilon_{\bar{\pi}})$ . When  $\pi$  is a union of SCCs,  $B_{\bar{\pi}\bar{\pi}}$  inherits its spectrum from a subset of  $B$ , so  $\det(I - B) \neq 0$  already implies invertibility.

A *soft cluster intervention* adds a deterministic offset  $\delta_\pi \in \mathbb{R}^{|\pi|}$  to the equations of  $X_\pi$ , replacing  $X_\pi = B_{\pi,V}X + \varepsilon_\pi$  with  $X_\pi = B_{\pi,V}X + \varepsilon_\pi + \delta_\pi$ . Soft interventions preserve the cyclic mechanism inside  $\pi$  and induce a cluster-level shift on  $G^{\text{sc}}$ .

**C-DAG identification.** Once  $G^{\text{sc}}$  is in hand, the C-DAG identification theorems of [2] apply directly: for clusters  $\pi_i, \pi_j$  of  $G^{\text{sc}}$ , the interventional distribution  $P(X_{\pi_j} \mid \text{do}(X_{\pi_i} = c))$  is identifiable from  $P(X)$  whenever the standard ID conditions hold on  $G^{\text{sc}}$ .

## 5 Experimental Results

We illustrate [Theorem 1](#) on synthetic linear non-Gaussian cyclic SCMs using the recipe of [19] from § 4.2. The interventional case ([Appendix A.1](#)) inherits the unmodified guarantees of [21] and is not explored empirically. All experiments ran on a single CPU workstation (AMD Ryzen 9 9950X, 128 GB RAM); fit times are reported in [Figure 4](#).

### 5.1 Setup

**Data-generating process.** We generate linear non-Gaussian cyclic SCMs on  $d = 10$  variables with a controlled number  $\kappa \in \{3, 4, 5\}$  of non-trivial SCCs and edge densities  $\lambda \in \{0.3, 0.5, 0.8\}$ . For each  $(d, \kappa, \lambda)$ , the  $d$  nodes are randomly partitioned into  $\kappa$  non-trivial SCCs (each of size  $\geq 2$ ) plus singleton nodes. Within each SCC a directed Hamilton cycle ensures mutual reachability and additional intra-SCC directed edges are sampled at probability  $\lambda$ . Between clusters, edges that respect a random topological order are sampled at probability  $\lambda$ . Edge weights are sampled in  $[0.5, 0.95]$  with random sign. Noise components  $\varepsilon_i$  are mutually independent and Laplace-distributed. Sample sizes  $n \in [50, 10^5]$ ; each cell is replicated across 10 random seeds.

Each configuration is run under two spectral-radius regimes: **Stable** ( $\rho(B) \approx 0.9$ ): the first-stable filter can recover the true  $B$ . **Unstable** ( $\rho(B) = 1.5$ ): the first-stable filter does not necessarily select the right equivalence-class member; by [Theorem 1](#) the condensation is the same.

**Method (deliberately broader than [Algorithm 1](#)).** [Algorithm 1](#) recovers  $G^{\text{sc}}$  from any single admissible permutation. For the experiments we instead run the full ICA-LiNG-D enumeration of [19] so that we can additionally report variable-level  $F_1$  and visualize the gap between the identifiable cluster-level structure and the unidentifiable intra-SCC structure. We pick the first-stable candidate (lowest-spectral-radius candidate if no stable one exists). By [Theorem 1](#), this choice does not affect the recovered  $\widehat{G}^{\text{sc}}$ . We use threshold  $\tau = 0.1$ ; sensitivity to this choice is reported in [Appendix C.2](#).

**Metrics.** Ground truth is the true SCC partition of  $G$  (Tarjan on the data-generating  $B$ ) and the corresponding condensation. All  $F_1$  scores are micro-averaged over directed edges. We report:

- *Adjusted Rand Index* (ARI) [14] of the predicted partition versus the true SCC partition;
- *cluster-DAG  $F_1$* :  $F_1$  of the predicted edges projected onto the true SCC partition against the edges of  $G^{\text{sc}}$  (the identifiable target of [Theorem 1](#));

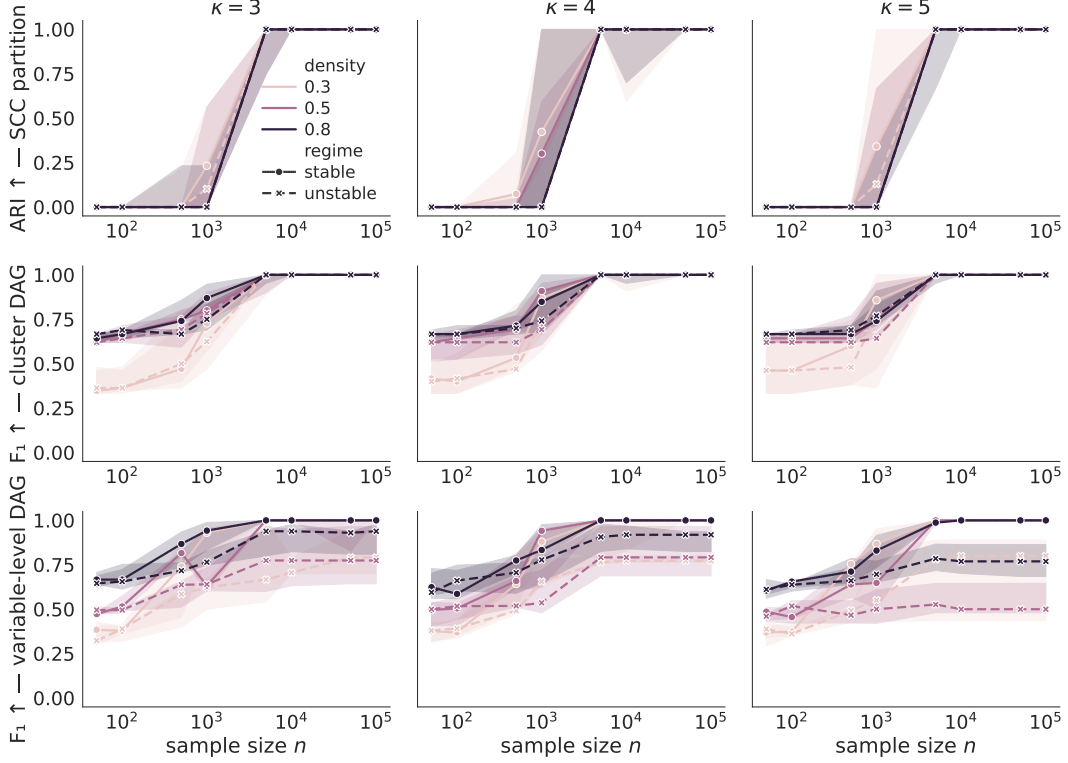


Figure 3: Synthetic-data evaluation of the first-stable ICA-LiNG-D recipe ( $d = 10$ , 10 seeds per cell). Columns: number of SCCs  $\kappa$ . Densities  $\lambda \in \{0.3, 0.5, 0.8\}$  in progressively darker shades. Solid: stable regime ( $\rho(B) \approx 0.9$ ); dashed: unstable ( $\rho(B) = 1.5$ ). Rows: ARI of the recovered partition; cluster-DAG  $F_1$ ; variable-level  $F_1$ . Shaded bands: 95% CI across seeds.

- *variable-level  $F_1$* :  $F_1$  over all directed edges (including intra-SCC), quantifying the gap between identifiable and unidentifiable structure.

## 5.2 Results

Figure 3 shows partition and edge recovery as functions of sample size for both regimes and all three densities, faceted by  $\kappa$ . Three observations:

- *Partition recovery*. ARI rises with  $n$  and approaches 1 in both regimes and at all densities, confirming consistency of LiNG-D + Tarjan under non-Gaussian noise.
- *Cluster-DAG  $F_1$* . Cluster-DAG  $F_1$  converges to 1 with  $n$  in both regimes, directly illustrating [Theorem 1](#):  $G^{\text{sc}}$  is identifiable regardless of the stability condition.
- *Variable-level  $F_1$* . In the stable regime (solid lines), the true  $B$  is the unique stable representative of its equivalence class, so the first-stable filter recovers it and variable-level  $F_1 \rightarrow 1$ . In the unstable regime (dashed), the true  $B$  has  $\rho(B) = 1.5$ , so the filter does not necessarily select the right member of the equivalence class and variable-level  $F_1$  saturates below 1. The gap is the unidentifiable intra-SCC structure.

The contrast between the two regimes is the key empirical message: the condensation (rows 1–2) is robustly recovered even when the variable-level graph (row 3) is not. This is the practical motivation for [§ 4.3](#): rather than chasing the unidentifiable intra-SCC structure, work at the cluster level if possible, where the C-DAG is fully recovered and standard C-DAG identification machinery applies.

## 5.3 Scalability vs disjoint-cycle baseline

We compare against [9]. Their identification target differs from ours: they recover the full variable-level adjacency under the assumption that all cycles in  $G$  are pairwise disjoint, using third-order

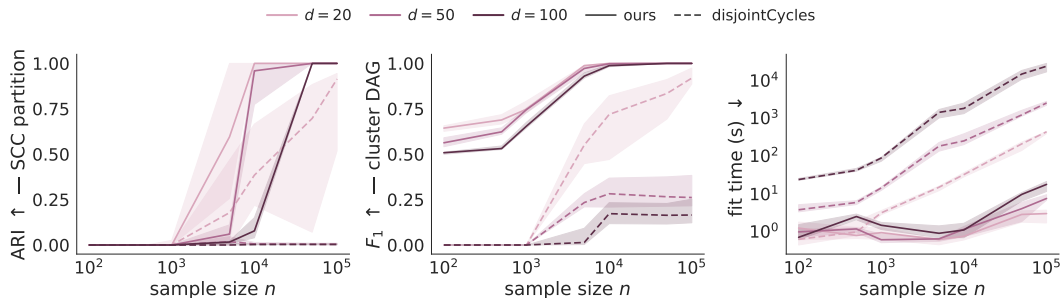


Figure 4: Scalability vs the disjoint-cycle baseline of [9] ( $d \in \{20, 50, 100\}$ ,  $\lambda = 0.5$ ,  $\kappa = 10$  SCCs, 10 seeds per cell).  $d$  encoded by colour intensity; solid: ours, dashed: disjointCycles. Left to right: ARI of the recovered partition, cluster-DAG  $F_1$ , fit time (s). Shaded bands: 95% CI across seeds.

moments rather than ICA, and their guarantees additionally require the noise distribution to be skewed. The comparison is not strictly fair—they solve a harder problem under stronger assumptions—but it is the closest baseline available, so we project both methods onto our cluster-level metrics. Their procedure already returns a cluster partition: the layered topological ordering has layers that are themselves SCCs (singletons or cycles), which we read directly as the predicted partition. Cluster-DAG  $F_1$  is then computed identically for both methods by projecting the variable-level adjacency onto the predicted partition.

We sweep  $d \in \{20, 50, 100\}$  at density  $\lambda = 0.5$  with  $\kappa = 10$ ,  $n \in [10^2, 10^5]$ , 10 seeds per cell<sup>3</sup>. Unlike the main experiments of § 5, which use symmetric Laplace noise, the scalability grid uses skewed exponential noise so that the baseline’s third-moment tests have nonzero signal; both methods operate inside their respective noise regimes. We run their procedure matching the configuration of their published simulations.

Figure 4 shows the result. Our method saturates cluster-DAG  $F_1$  at  $n \geq 10^4$  for every  $d$ ; ARI saturates at  $n \geq 10^5$ . The baseline recovers the partition only at  $d = 20$  and plateaus below 0.3 in cluster-DAG  $F_1$  for  $d \in \{50, 100\}$  even at  $n = 10^5$ . Fit time grows steeply for the baseline, reaching  $10^4$  s per seed at  $n = 10^5$ ,  $d = 100$ , while ours stays within  $10^1$  s—consistent with the  $\mathcal{O}(kn d^2 + d^3)$  bound of Theorem 2.

## 6 Discussion

We have extended the coarsening framework of [21] to directed graphs with cycles, with the SCC partition as the lattice floor and the condensation  $G^{\text{sc}}$  as the canonical identification target. Theorem 1 refines the cyclic-SCM identifiability picture of [19]: although the underlying micro-graph is identifiable only up to a distributional equivalence class,  $G^{\text{sc}}$  is fully identifiable from the observational distribution, supplying the prerequisite of the C-DAG identification machinery of [2].

The observational approach requires linear non-Gaussian noise and no latent confounders, but with the practical advantage of requiring no interventional data. Hard do-interventions on a single variable inside a non-trivial SCC sever the cyclic mechanism and are excluded throughout; only soft (shift) interventions and hard interventions on entire SCCs are well-defined in the cyclic SCM setting (§ 4.3).

**Open directions.** (i) Latent-confounder generalisations via overcomplete ICA [30, 7]: the cycle-reversal argument carries over because cycle reversals are purely a graph-level operation, independent of the source/observed dimension. (ii) Mixed-Gaussian extension—ICA’s rotational ambiguity in the Gaussian subspace is global, not per-SCC: with two Gaussian sources in different SCCs, an orthogonal rotation can mix them, introducing inter-SCC entries in the equivalent demixing matrix and falsely merging the two SCCs in the recovered condensation. The condensation-invariance argument therefore survives only when at most one noise source is Gaussian *overall*; lifting this restriction would address the open problem of [19, § 6] on Gaussian/non-Gaussian mixtures and

<sup>3</sup>Our generator can nonetheless create overlapping cycles inside each SCC of size  $\geq 3$ . This does not satisfy [9] assumption and might explain the results. See Appendix C.1.

likely requires structural side information beyond ICA. (iii) Empirical cluster-level causal-effect estimation, applying the C-DAG ID algorithm of [2] to a recovered  $\widehat{G}^{\text{sc}}$  on real data.

## Acknowledgments and Disclosure of Funding

The work of FM and FCP was supported by Novo Nordisk Foundation grant number NNF23OC0085356. The work by AM was supported by Novo Nordisk Foundation grant number NNF20OC0062897. The authors thank Carlos Lima Azevedo and Serio Angelo Maria Agriesti for helpful discussions and feedback.

## References

- [1] Carlos Améndola, Philipp Dettling, Mathias Drton, Federica Onori, and Jun Wu. Structure learning for cyclic linear causal models. In *Conference on Uncertainty in Artificial Intelligence*, pages 999–1008. PMLR, 2020.
- [2] Tara V. Anand, Adèle H. Ribeiro, Jin Tian, and Elias Bareinboim. Causal effect identification in cluster DAGs. In *AAAI Conference on Artificial Intelligence*, 2023.
- [3] Sander Beckers and Joseph Y. Halpern. Abstracting causal models. In *AAAI Conference on Artificial Intelligence*, 2019.
- [4] John Adrian Bondy and U. S. R. Murty. *Graph Theory with Applications*. Elsevier, New York, 1976.
- [5] Stephan Bongers, Patrick Forré, Jonas Peters, and Joris M. Mooij. Foundations of structural causal models with cycles and latent variables. *Annals of Statistics*, 49(5):2885–2915, 2021.
- [6] Aiyou Chen and Peter J. Bickel. Consistent independent component analysis and prewhitening. *IEEE Transactions on Signal Processing*, 53(10):3625–3632, 2005.
- [7] Haoyue Dai, Immanuel Albrecht, Peter Spirtes, and Kun Zhang. Distributional equivalence in linear non-Gaussian latent-variable cyclic causal models: Characterization and learning. In *International Conference on Learning Representations (ICLR)*, 2026.
- [8] Philipp Dettling, Mathias Drton, and Mladen Kolar. On the lasso for graphical continuous Lyapunov models. In Francesco Locatello and Vanessa Didelez, editors, *Proceedings of the Third Conference on Causal Learning and Reasoning*, volume 236 of *Proceedings of Machine Learning Research*, pages 514–550. PMLR, 01–03 Apr 2024.
- [9] Mathias Drton, Marina Garrote-López, Niko Nikov, Elina Robeva, and Y. Samuel Wang. Causal discovery for linear non-Gaussian models with disjoint cycles. In Silvia Chiappa and Sara Magliacane, editors, *Proceedings of the Forty-first Conference on Uncertainty in Artificial Intelligence*, volume 286 of *Proceedings of Machine Learning Research*, pages 1064–1083. PMLR, 21–25 Jul 2025.
- [10] Doris Entner and Patrik O Hoyer. Estimating a causal order among groups of variables in linear models. In *International Conference on Artificial Neural Networks*, pages 84–91. Springer, 2012.
- [11] Jan Eriksson and Visa Koivunen. Identifiability, separability, and uniqueness of linear ICA models. *IEEE Signal Processing Letters*, 11(7):601–604, 2004.
- [12] Patrick Forré and Joris M. Mooij. Constraint-based causal discovery for non-linear structural causal models with cycles and latent confounders. In *Conference on Uncertainty in Artificial Intelligence (UAI)*, 2018.
- [13] Niels Hansen and Alexander Sokol. Causal interpretation of stochastic differential equations. *Electronic Journal of Probability*, 19:1–24, 2014.
- [14] Lawrence Hubert and Phipps Arabie. Comparing partitions. *Journal of Classification*, 2(1):193–218, 1985.

- [15] Aapo Hyvärinen. Fast and robust fixed-point algorithms for independent component analysis. *IEEE Transactions on Neural Networks*, 10(3):626–634, 1999.
- [16] Aapo Hyvärinen, Juha Karhunen, and Erkki Oja. *Independent Component Analysis*. John Wiley & Sons, May 2001.
- [17] Yoshinobu Kawahara, Kenneth Bollen, Shohei Shimizu, and Takashi Washio. GroupLiNGAM: Linear non-Gaussian acyclic models for sets of variables. *arXiv preprint arXiv:1006.5041*, 2010.
- [18] Harold W. Kuhn. The Hungarian method for the assignment problem. *Naval Research Logistics Quarterly*, 2(1–2):83–97, 1955.
- [19] Gustavo Lacerda, Peter Spirtes, Joseph Ramsey, and Patrik O. Hoyer. Discovering cyclic causal models by independent components analysis. In *Conference on Uncertainty in Artificial Intelligence (UAI)*, 2008.
- [20] Michael S. Lewicki and Terrence J. Sejnowski. Learning overcomplete representations. *Neural Computation*, 12(2):337–365, 2000.
- [21] Francisco Madaleno, Pratik Misra, and Alex Markham. Coarsening causal DAG models. In Bijan Mazaheri and Niels Richard Hansen, editors, *Proceedings of the Fifth Conference on Causal Learning and Reasoning*, Proceedings of Machine Learning Research. PMLR, Apr 2026.
- [22] Takashi N. Maeda and Shohei Shimizu. RCD: Repetitive causal discovery of linear non-Gaussian acyclic models with latent confounders. In *International Conference on Artificial Intelligence and Statistics (AISTATS)*, 2020.
- [23] Jari Miettinen, Klaus Nordhausen, Hannu Oja, and Sara Taskinen. Fourth moments and independent component analysis. *Statistical Science*, 30(3):372–390, 2015.
- [24] Joris M. Mooij, Dominik Janzing, and Bernhard Schölkopf. From ordinary differential equations to structural causal models: the deterministic case. In *Proceedings of the Twenty-Ninth Conference on Uncertainty in Artificial Intelligence*, UAI’13, page 440–448. AUAI Press, 2013.
- [25] Cecilie Olesen Recke and Niels Richard Hansen. Identifiability and estimation in continuous Lyapunov models. *arXiv preprint arXiv:2603.17142*, 2026.
- [26] Cecilie Olesen Recke, Sarah Lumpp, Nataliia Kushnerchuk, Janike Oldekop, Jiayi Li, Jane Ivy Coons, and Elina Robeva. Identifiability in graphical discrete Lyapunov models. *arXiv preprint arXiv:2601.21818*, 2026.
- [27] Dominik Rothenhäusler, Christina Heinze, Jonas Peters, and Nicolai Meinshausen. Backshift: Learning causal cyclic graphs from unknown shift interventions. *Advances in neural information processing systems*, 28, 2015.
- [28] Paul K. Rubenstein, Sebastian Weichwald, Stephan Bongers, Joris M. Mooij, Dominik Janzing, Moritz Grosse-Wentrup, and Bernhard Schölkopf. Causal consistency of structural equation models. In *Conference on Uncertainty in Artificial Intelligence (UAI)*, 2017.
- [29] Karen Sachs, Omar Perez, Dana Pe’er, Douglas A. Lauffenburger, and Garry P. Nolan. Causal protein-signaling networks derived from multiparameter single-cell data. *Science*, 308(5721):523–529, 2005.
- [30] Saber Salehkaleybar, Amiremad Ghassami, Negar Kiyavash, and Kun Zhang. Learning linear non-Gaussian causal models in the presence of latent variables. *Journal of Machine Learning Research*, 21(39):1–24, 2020.
- [31] Ehsan Sharifian, Saber Salehkaleybar, and Negar Kiyavash. Near-optimal experiment design in linear non-Gaussian cyclic models. In D. Belgrave, C. Zhang, H. Lin, R. Pascanu, P. Koniusz, M. Ghassemi, and N. Chen, editors, *Advances in Neural Information Processing Systems*, volume 38, pages 63520–63538. Curran Associates, Inc., 2025.

- [32] Shohei Shimizu, Patrik O. Hoyer, Aapo Hyvärinen, and Antti Kerminen. A linear non-Gaussian acyclic model for causal discovery. *Journal of Machine Learning Research*, 7:2003–2030, 2006.
- [33] Shohei Shimizu, Takanori Inazumi, Yasuhiro Sogawa, Aapo Hyvärinen, Yoshinobu Kawahara, Takashi Washio, Patrik O. Hoyer, and Kenneth Bollen. DirectLiNGAM: A direct method for learning a linear non-Gaussian structural equation model. *Journal of Machine Learning Research*, 12:1225–1248, 2011.
- [34] Peter Spirtes. Directed cyclic graphical representations of feedback models. In *Conference on Uncertainty in Artificial Intelligence (UAI)*, 1995.
- [35] Robert Tarjan. Depth-first search and linear graph algorithms. *SIAM Journal on Computing*, 1(2):146–160, 1972.
- [36] Daniele Tramontano, Anthea Monod, and Mathias Drton. Learning linear non-gaussian polytree models. In *Uncertainty in Artificial Intelligence*, pages 1960–1969. PMLR, 2022.
- [37] Gherardo Varando and Niels Richard Hansen. Graphical continuous Lyapunov models. In Jonas Peters and David Sontag, editors, *Proceedings of the 36th Conference on Uncertainty in Artificial Intelligence (UAI)*, volume 124 of *Proceedings of Machine Learning Research*, pages 989–998. PMLR, 03–06 Aug 2020.
- [38] Jonas Wahl, Urmi Ninad, and Jakob Runge. Foundations of causal discovery on groups of variables. *Journal of Causal Inference*, 12(1):20230041, 2024.

## A Additional Comments

### A.1 On Interventional Extensions

Under soft interventions, the cyclic SCM becomes  $X^I = (I - B)^{-1}(\varepsilon + \delta)$ , so intervention effects propagate through the whole graph, including back through cycles. Nodes within the same SCC are mutual ancestors and therefore share identical intervened-ancestor signatures, so the `RefineTest` of [21] cannot split an SCC: `RePaRe` recovers  $G^{\text{sc}}$  with the SCC partition as its floor without modification.

## B Additional Proofs

### B.1 Proof of Theorem 2

*Proof.* The overall time complexity of [Algorithm 1](#) is governed by the sequential execution of statistical estimation and graph-theoretic aggregation. We break down the worst-case asymptotic time complexity by stage:

**Independent Component Analysis (FastICA):** FastICA computes the unmixing matrix  $\hat{W}$  iteratively. The computational cost per iteration is dominated by matrix multiplications involving the  $n \times d$  data matrix, taking  $\mathcal{O}(k \cdot n \cdot d^2)$  time, where  $k$  represents the number of iterations until convergence.

**Admissible-permutation search (combinatorial bypass).** A candidate adjacency requires a row permutation  $P$  making the diagonal of  $P\hat{W}$  nonzero. Exhaustive enumeration over the distributional equivalence class incurs an  $N$ -rooks worst-case cost of  $\mathcal{O}(d!)$  (in practice typically much smaller, depending on sparsity of  $\hat{W}$ ). By [Theorem 1](#), any admissible  $P$  yields the same  $G^{\text{sc}}$ , so finding one  $P$  suffices: solving a single perfect matching with the Hungarian algorithm runs in  $\mathcal{O}(d^3)$ .

**Candidate Generation and Thresholding:** Once an admissible permutation  $P$  is found, computing  $\hat{B}_P = I - \text{diag}(P\hat{W})^{-1}P\hat{W}$  and applying element-wise thresholding takes  $\mathcal{O}(d^2)$  time. If optional stability filtering is applied, computing the spectral radius  $\rho(\hat{B}_P)$  via eigenvalue decomposition bounds this step at  $\mathcal{O}(d^3)$ .

**SCC Partitioning:** Extracting the Strongly Connected Components via Tarjan’s algorithm runs in linear time with respect to the candidate graph’s vertices and edges, taking  $\mathcal{O}(d + |E|) \subseteq \mathcal{O}(d^2)$  time.

**Condensation Edge Formation:** Scanning the edge list to establish inter-cluster adjacencies requires a single pass over the nonzero elements of the adjacency matrix, taking  $\mathcal{O}(|E|) \subseteq \mathcal{O}(d^2)$  time.

Summing these stages yields an overall worst-case time complexity strictly bounded by  $\mathcal{O}(k \cdot n \cdot d^2 + d^3)$ .  $\square$

## B.2 Transitive closure and SCCs

For a directed graph  $G = (V, E)$ , denote the existence of a directed path from vertex  $u$  to vertex  $v$  by the reachability relation  $u \rightsquigarrow_G v$ . By convention, a vertex can always reach itself (paths of length 0), so  $u \rightsquigarrow_G u$  for all  $u \in V$ .

**Definition 3** (Strongly connected component). *Define a binary relation  $\sim_G$  on  $V$  by*

$$u \sim_G v \iff (u \rightsquigarrow_G v) \wedge (v \rightsquigarrow_G u).$$

*The relation  $\sim_G$  is an equivalence relation (reflexive, symmetric, transitive). A strongly connected component (SCC) of  $G$  is an equivalence class of  $V$  under  $\sim_G$ .*

The following result provides an alternative route to condensation identifiability via the mixing matrix  $A = (I - B)^{-1}$  and its transitive-closure interpretation. While the main proof of [Theorem 1](#) uses the more direct cycle-reversal argument, the transitive-closure perspective is independently useful—for instance, it connects to the path-rank lemma of [\[7\]](#) and to settings where one works with  $A$  rather than  $W$ .

**Definition 4** (Transitive closure). *The transitive closure of a directed graph  $G = (V, E)$  is the graph  $G^{\text{tc}} = (V, E^{\text{tc}})$  with edge set*

$$E^{\text{tc}} = \{(u, v) \in V \times V \mid u \rightsquigarrow_G v\}.$$

**Theorem 3** (SCCs are preserved under transitive closure). *Let  $G = (V, E)$  be a directed graph and let  $G^{\text{tc}} = (V, E^{\text{tc}})$  be its transitive closure. Then  $G$  and  $G^{\text{tc}}$  have the same SCCs.*

*Proof.* It suffices to show  $u \sim_G v \iff u \sim_{G^{\text{tc}}} v$  for all  $u, v \in V$ .

( $\Rightarrow$ ) Suppose  $u \sim_G v$ , so  $u \rightsquigarrow_G v$  and  $v \rightsquigarrow_G u$ . By [Definition 4](#),  $(u, v) \in E^{\text{tc}}$  and  $(v, u) \in E^{\text{tc}}$ , hence  $u \rightsquigarrow_{G^{\text{tc}}} v$  and  $v \rightsquigarrow_{G^{\text{tc}}} u$ , i.e.  $u \sim_{G^{\text{tc}}} v$ .

( $\Leftarrow$ ) Suppose  $u \sim_{G^{\text{tc}}} v$ , so there is a path  $u = x_0, x_1, \dots, x_k = v$  in  $G^*$ . Each step  $(x_i, x_{i+1}) \in E^{\text{tc}}$  implies  $x_i \rightsquigarrow_G x_{i+1}$  by [Definition 4](#). Transitivity of  $\rightsquigarrow_G$  then gives  $u \rightsquigarrow_G v$ . Symmetric reasoning yields  $v \rightsquigarrow_G u$ , so  $u \sim_G v$ .

The two implications give equality of equivalence classes, hence equality of SCCs.  $\square$

**Remark.** [Theorem 3](#) means that if one recovers  $\text{supp}(A) = \text{adjacency}(G^{\text{tc}})$ —the transitive closure of  $G$ —from the mixing matrix  $A = (I - B)^{-1}$ , the SCC partition extracted from it is exactly the SCC partition of  $G$ . This provides an alternative proof route for the SCC-partition part of [Theorem 1](#), going through  $A$  rather than  $W$ . The main text uses the cycle-reversal argument because it also immediately handles inter-SCC edges without requiring a separate step.

## B.3 Sample complexity for exact condensation recovery

[Corollary 1](#) guarantees that [Algorithm 1](#) returns the correct condensation *in the large-sample limit*. This subsection turns that asymptotic statement into a finite-sample bound on the sample complexity, that is, how many observations  $n$  are sufficient to exactly recover  $G^{\text{sc}}$  with probability at least  $1 - \delta$ .

**Setup.** Fix a linear non-Gaussian SCM  $X = BX + \varepsilon$  with mutually independent noise components, at most one Gaussian, and  $\det(I - B) \neq 0$ . Let

$$\beta_{\min} := \min_{(i,j): B_{ij} \neq 0} |B_{ij}|$$

denote the smallest nonzero entry of the data-generating  $B$ . Let  $\hat{W}_n$  be the FastICA estimate from  $n$  i.i.d. samples and let  $\hat{B}_n$  be the candidate produced by [Algorithm 1](#) at threshold  $\tau_n$ .

**Proposition 3** (Finite-sample exact recovery). *Assume the noise components have bounded fourth moments. There exist constants  $K_1, K_2 > 0$  depending on  $B$  and the noise distribution such that, for any threshold sequence  $\tau_n$  with*

$$\tau_n \rightarrow 0, \quad \sqrt{n} \tau_n \rightarrow \infty, \quad \tau_n < \frac{\beta_{\min}}{2} \text{ for all sufficiently large } n,$$

*the recovered condensation satisfies*

$$\Pr[\hat{G}_n^{\text{sc}} \neq G^{\text{sc}}] \leq \Pr[\text{supp}(\hat{B}_n) \neq \text{supp}(B)] \leq \frac{K_1}{n^2 (\beta_{\min} - \tau_n)^4} + \frac{K_2}{n^2 \tau_n^4}. \quad (3)$$

*The two terms correspond exactly to the two failure modes of [Proposition 2](#): the first to dropping a true edge (Mode (a), splitting an SCC), the second to keeping a spurious entry (Mode (b), merging two SCCs).*

*Proof.* The argument has three steps.

*Step 1 (entry-wise rates for  $\hat{B}$ ).* Under bounded fourth moments and at most one Gaussian source, FastICA is  $\sqrt{n}$ -consistent for the unmixing matrix up to its canonical row-permutation/sign indeterminacy: with  $\Pi$  a permutation and  $D$  a diagonal sign matrix aligning  $\hat{W}_n$  with  $W^*$ ,  $\sqrt{n}(\hat{W}_n - W^*\Pi D)$  is asymptotically normal with finite covariance [6, 23], and bounded fourth moments of the noise transfer to bounded fourth moments of each entry of  $\sqrt{n}(\hat{W}_n - W^*\Pi D)$ . Hence there exists  $M > 0$  such that

$$\mathbb{E}[(\hat{W}_{n,ij} - W_{ij}^*)^4] \leq \frac{M}{n^2}$$

for all entries  $(i, j)$  and all  $n$  large enough.

The map  $W \mapsto I - \text{diag}(PW)^{-1}PW$  used in Algorithm 1 is smooth on the open set  $\{M : (PM)_{ii} \neq 0 \forall i\}$  but has singularities on its boundary, so it is not globally Lipschitz. We therefore localize via a high-probability event. Pick a closed ball  $\mathcal{N}$  of radius  $r > 0$  around  $W^*$  on which the map is  $L$ -Lipschitz (such an  $L$  exists by smoothness on the compact  $\mathcal{N}$ , with  $r, L$  depending only on  $B$ ), and define

$$\mathcal{E}_n := \{ \hat{W}_n \in \mathcal{N} \}.$$

By Markov's inequality applied to the fourth moment of  $\|\hat{W}_n - W^*\|_\infty$  and a union bound over the at most  $d^2$  entries,

$$\Pr[\mathcal{E}_n^c] \leq \frac{d^2 M}{n^2 r^4}.$$

Outside this event we have no control on  $\hat{B}_n$ , but the event itself is rare. Inside it, the Lipschitz bound gives  $|\hat{B}_{n,ij} - B_{ij}| \leq L \|\hat{W}_n - W^*\|_\infty$ , so for any  $t > 0$  a union bound over entries combined with Markov on the fourth moment of  $\hat{W}$  yields

$$\Pr[\{|\hat{B}_{n,ij} - B_{ij}| > t\} \cap \mathcal{E}_n] \leq \frac{d^2 L^4 M}{n^2 t^4}.$$

Combining the two contributions,

$$\Pr[|\hat{B}_{n,ij} - B_{ij}| > t] \leq \frac{d^2 L^4 M}{n^2 t^4} + \frac{d^2 M}{n^2 r^4}.$$

Under the hypothesis  $\tau_n \rightarrow 0$  and  $\tau_n < \frac{\beta_{\min}}{2}$ , both relevant deviations  $t \in \{\beta_{\min} - \tau_n, \tau_n\}$  stay bounded above by a fixed constant for all large  $n$ , so the second summand is absorbed into the first up to a multiplicative constant: there exists  $K > 0$  (depending on  $B$  and the noise) such that, for all  $n$  large enough and all  $t \in \{\beta_{\min} - \tau_n, \tau_n\}$ ,

$$\Pr[|\hat{B}_{n,ij} - B_{ij}| > t] \leq \frac{K}{n^2 t^4}.$$

*Step 2 (support recovery via two opposing tails).*

- *False negative.* A true edge  $|B_{ij}| \geq \beta_{\min}$  is dropped, i.e.  $|\hat{B}_{n,ij}| < \tau_n$ . By the triangle inequality this requires  $|\hat{B}_{n,ij} - B_{ij}| > \beta_{\min} - \tau_n$ , and Step 1 bounds the probability by  $\frac{K}{n^2 (\beta_{\min} - \tau_n)^4}$ .
- *False positive.* A true non-edge  $B_{ij} = 0$  is kept, i.e.  $|\hat{B}_{n,ij}| \geq \tau_n$ . By Step 1 this has probability at most  $\frac{K}{(n^2 \tau_n^4)}$ .

A union bound over the at most  $d^2$  entries gives

$$\Pr[\text{supp}(\hat{B}_n) \neq \text{supp}(B)] \leq \frac{d^2 K}{n^2 (\beta_{\min} - \tau_n)^4} + \frac{d^2 K}{n^2 \tau_n^4},$$

absorbing  $d^2 K$  into  $K_1, K_2$ .

*Step 3 (from  $\text{supp}(B)$  to the condensation).* Once  $\text{supp}(\hat{B}_n) = \text{supp}(B)$ , the directed graph induced by  $\hat{B}_n$  is exactly  $G$ , so Tarjan's algorithm returns the exact SCC partition and the exact condensation. This step is deterministic, hence

$$\Pr[\hat{G}_n^{\text{sc}} \neq G^{\text{sc}}] \leq \Pr[\text{supp}(\hat{B}_n) \neq \text{supp}(B)],$$

which combined with Step 2 yields (3).  $\square$

**Sample complexity.** The two terms in (3) are balanced when  $\tau_n = \frac{\beta_{\min}}{2}$ , in which case both reduce to a constant times  $\frac{1}{(n^2 \beta_{\min}^4)}$ . Inverting the bound yields:

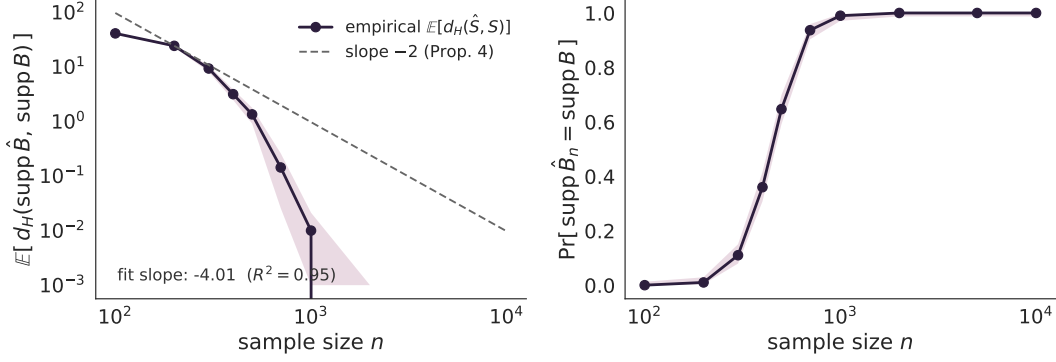


Figure 5: Empirical corroboration of [Proposition 3](#) on the main-grid setup ( $d = 10$ ,  $\kappa = 4$ ,  $\lambda = 0.5$ ,  $\beta_{\min} \approx 0.51$ ,  $\tau = \frac{\beta_{\min}}{2}$ , 300 seeds per cell). **Left:**  $\mathbb{E}[d_H(\text{supp } \hat{B}, \text{supp } B)]$  vs  $n$  on log-log; the dashed reference line has the predicted slope  $-2$  and the empirical slope is steeper, consistent with the bound being a conservative upper bound under Laplace noise. **Right:**  $\Pr[\text{supp } \hat{B}_n = \text{supp } B]$  vs  $n$  with 95% CI bands; the slope in the transition window  $n \in [200, 1000]$  is  $-2.9$ . Recovery is exact in every seed at  $n \geq 2000$ .

**Corollary 2** (Sample complexity). *Under the assumptions of [Proposition 3](#), fix the threshold to  $\tau = \frac{\beta_{\min}}{2}$ . Then for any target error level  $\delta \in (0, 1)$ , taking*

$$n \geq \frac{4}{\beta_{\min}^2} \sqrt{\frac{K_1 + K_2}{\delta}}$$

*samples is sufficient for*

$$\Pr[\hat{G}_n^{\text{sc}} = G^{\text{sc}}] \geq 1 - \delta.$$

*Proof.* Substitute  $\tau_n = \frac{\beta_{\min}}{2}$  into (3): the sum of the two terms is bounded by  $\frac{16(K_1 + K_2)}{n^2 \beta_{\min}^4}$ . Requiring this to be at most  $\delta$  and solving for  $n$  gives the stated bound.  $\square$

Three remarks on [Corollary 2](#). First, the sample complexity scales as  $n \asymp \frac{d}{\beta_{\min}^2 \sqrt{\delta}}$  once the polynomial-in- $d$  factor inside  $K_1, K_2$  (namely  $K_i \asymp d^2$ ) is unpacked—linear in the dimension and quadratic in the inverse minimum-edge magnitude, with  $\frac{1}{\sqrt{\delta}}$  dependence on the failure probability. Stronger noise tails (e.g. sub-Gaussian) would replace the polynomial  $\delta$ -dependence with  $\log(\frac{1}{\delta})$  via a Hoeffding-type bound, but bounded fourth moments alone yield the polynomial rate above. Second, the choice  $\tau = \frac{\beta_{\min}}{2}$  requires a priori knowledge of  $\beta_{\min}$ , which we do not have in practice; the alternative  $\tau_n \asymp n^{-\frac{1}{4}}$  (any sequence with  $\tau_n \rightarrow 0$  and  $\sqrt{n} \tau_n \rightarrow \infty$ ) gives a  $\frac{1}{n}$  rate instead of  $\frac{1}{n^2}$  but is robust to misspecification of  $\beta_{\min}$ . Third, the bound (3) reproduces the threshold-sensitivity picture of [Appendix C.2](#) term by term: the failure modes of [Proposition 2](#) are exactly the two error events that the union bound in Step 2 controls.

**Empirical corroboration.** [Figure 5](#) reports a Monte-Carlo experiment that tests the rate of [Proposition 3](#) on the same data-generating regime as the main-grid experiments of [§ 5](#) ( $d = 10$ ,  $\kappa = 4$  non-trivial SCCs,  $\lambda = 0.5$ , weights uniform in  $[0.5, 0.95]$ , Laplace noise;  $\beta_{\min} \approx 0.51$ ). We fix one ground-truth SCM, threshold at  $\tau = \frac{\beta_{\min}}{2}$  as prescribed by [Corollary 2](#), and over 300 independent seeds per cell sweep  $n \in [10^2, 10^5]$  on a log-spaced grid. The left panel plots  $\mathbb{E}[d_H(\text{supp } \hat{B}, \text{supp } B)]$ , a smooth proxy for the entry-wise tail probability. The right panel plots the binary exact-recovery probability  $\Pr[\text{supp } \hat{B} = \text{supp } B]$  with 95% CI bands. An Ordinary Least Squares (OLS) log-log fit on the cells with non-trivial failure rate gives empirical slopes of  $-4.0$  for mean Hamming distance and  $-2.9$  for exact-recovery error in the transition window, both steeper than the  $-2$  predicted by [Proposition 3](#). This is consistent with the proposition: the bound (3) is an upper bound under bounded fourth moments alone, and Laplace noise has faster-than-polynomial tails so the actual decay can be sharper. Recovery is exact in every seed by  $n = 2000$ .

#### B.4 Proof of [Proposition 2](#)

*Proof.* (a) Each non-trivial SCC contains at least one directed cycle. Removing any edge that lies on every cycle of an SCC disconnects the strong-connectivity relation on that SCC, partitioning it into smaller SCCs. (b) A

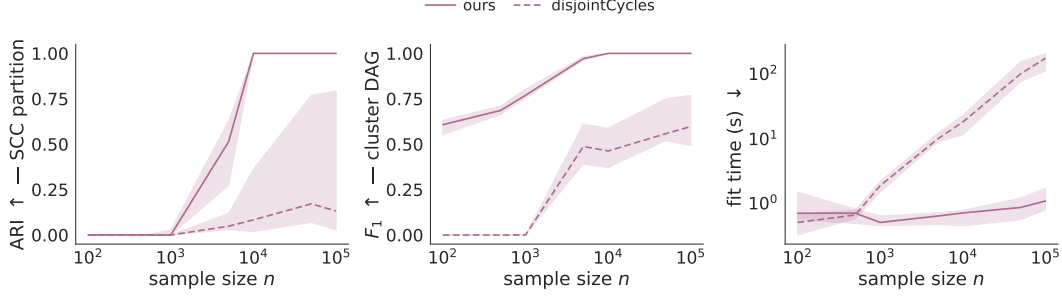


Figure 6: Strict disjoint-cycles micro experiment ( $d = 20$ ,  $\kappa = 5$ , every SCC a single Hamilton cycle,  $\lambda = 0.5$  inter-block, 10 seeds per cell). Solid: ours. Dashed: disjointCycles [9]. Left to right: ARI of the recovered partition, cluster-DAG  $F_1$ , fit time (s, log). Shaded bands: 95% CI across seeds.

spurious edge  $\hat{B}_{ij} \neq 0$  with  $i \in \pi$ ,  $j \in \pi'$  in the estimated graph, together with a path  $\pi' \rightsquigarrow \pi$  already present in  $G$ , closes a directed cycle through the two clusters and merges them.  $\square$

## C Additional Results

### C.1 Strict disjoint-cycles micro experiment

The main scalability sweep of § 5.3 at density  $\lambda = 0.5$ , creates multiple overlapping cycles within each SCC of size  $\geq 3$ , violating the disjoint-cycles assumption of [9]. To isolate the effect of that violation from the methodological gap, we run a complementary comparison whose data-generating process satisfies the assumption *exactly* by construction.

**Setup.** We fix  $d = 20$  with  $\kappa = 5$  non-trivial SCCs, inter-block density  $\lambda = 0.5$ , and *zero* intra-SCC chord density: each SCC is generated as a single directed Hamilton cycle and no further intra-SCC edges are added. Inter-block edges respect a random DAG ordering over the  $\kappa = 5$  blocks. By construction, every directed simple cycle in the resulting graph lies inside a single SCC and is the unique cycle of that SCC, so all simple cycles are pairwise vertex-disjoint, which is the structural premise of [9]. We sweep  $n \in [10^2, 10^5]$  with 10 seeds per cell, in the stable weight regime ( $w \in [0.5, 0.95]$ ,  $\rho(B) < 1$ ), and use skewed exponential noise so that the baseline’s third-moment tests carry signal. Both methods use the same fit configuration as the main scalability sweep.

**Results.** Figure 6 reports ARI of the recovered partition, cluster-DAG  $F_1$ , and fit time. Our method saturates at ARI = 1 and cluster-DAG  $F_1 = 1$  from  $n \geq 10^4$ , with fit time staying within  $\sim 1$  s across the full sweep. The disjoint-cycles baseline plateaus at median ARI  $\approx 0.13$  and median cluster-DAG  $F_1 \approx 0.60$  even at  $n = 10^5$ , with fit time growing to  $10^2$  s.

Inspection of the baseline’s predicted partitions explains the gap: at  $n \leq 10^3$ , every seed returns the trivial all-singletons partition (the procedure’s third-moment cycle tests at  $\alpha = 0.01$  have insufficient power and confirm no cycle); at  $n \geq 10^4$ , the output either contains seeds where some 2–3-cycles are correctly recovered and seeds where it merges most variables into a single cycle.

### C.2 Threshold sensitivity and the two failure modes

Algorithm 1 requires a threshold  $\tau > 0$  on  $|\hat{B}_{ij}|$ . Proposition 2 characterises two opposite failure modes; this subsection probes both empirically. We fix  $d = 10$ ,  $\kappa = 4$ ,  $\lambda = 0.5$  in the stable regime ( $\rho(B) < 1$ ) and sweep  $\tau$  across three orders of magnitude on a synthetic grid with 10 seeds per cell. The number of non-trivial SCCs is exactly  $\kappa = 4$  in every seed, but the singletons absorbed into non-trivial SCCs vary, so the true partition size  $|\Pi|$  ranges over  $\{4, 5, 6\}$  across seeds (median 5).

**Metrics.** Figure 7 reports three quantities. The first two are the same metrics used in § 5: ARI of the recovered SCC partition (left) and  $F_1$  of the recovered cluster-DAG edges (middle). The third is the size  $|\hat{\Pi}|$  of the estimated partition (right)—the failure modes:

- $|\hat{\Pi}| = 1$  (everything in one cluster): spurious entries above  $\tau$  closed paths between distinct true SCCs and merged everything (Mode (b) of Proposition 2).
- $|\hat{\Pi}| = d = 10$  (every variable is a singleton): true intra-SCC edges fell below  $\tau$  and every SCC splintered (Mode (a)).

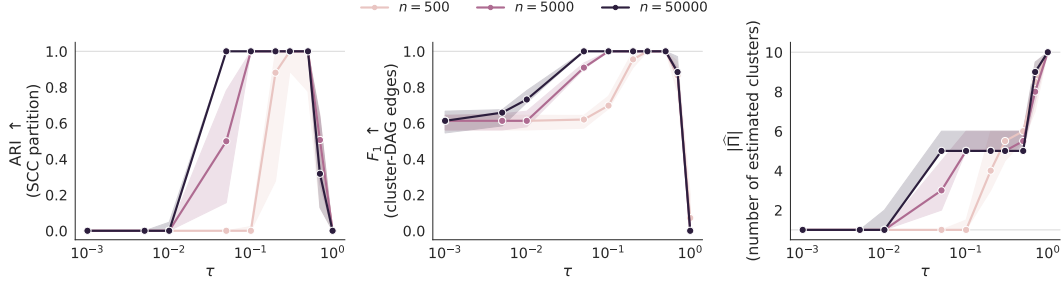


Figure 7: Threshold sensitivity at  $d = 10$ ,  $\kappa = 4$ ,  $\lambda = 0.5$  (stable regime, 10 seeds). **Left:** ARI of the recovered SCC partition. **Middle:**  $F_1$  of the recovered cluster-DAG edges. **Right:** number of estimated clusters  $|\hat{\Pi}|$ ; the true  $|\Pi|$  varies by seed across  $\{4, 5, 6\}$  with median 5, and inside the safe band  $|\hat{\Pi}|$  matches the per-seed truth. Curves are coloured by sample size. The right panel makes the two failure modes of Proposition 2 explicit:  $\tau \rightarrow 0$  collapses to  $|\hat{\Pi}| = 1$  (Mode (b)) and  $\tau \rightarrow 1$  saturates at  $|\hat{\Pi}| = d = 10$  (Mode (a)). Shaded bands: 95% CI across seeds.

- $|\hat{\Pi}| \in \{4, 5, 6\}$  (the  $\tau$ -independent range of the truth): the recovered partition agrees with the per-seed truth.

**Results.** At  $n \geq 5000$  the safe band is wide and roughly  $\tau \in [0.1, 0.5]$ : ARI = 1 and  $F_1 = 1$  in every seed and  $|\hat{\Pi}|$  matches the per-seed truth. Outside that band the figure shows the two failure modes unambiguously: at  $\tau \leq 0.01$  the right panel collapses to  $|\hat{\Pi}| = 1$ , at  $\tau = 1$  it climbs to  $|\hat{\Pi}| = d = 10$ , and ARI /  $F_1$  collapse correspondingly. The plateau begins later as  $n$  shrinks (at  $n = 500$  it begins only at  $\tau \geq 0.2$ ), reflecting the larger finite-sample fluctuations of  $\hat{B}$ . The default  $\tau = 0.1$  used throughout § 5 sits well inside the safe band whenever  $n \geq 5000$ .<sup>4</sup>

<sup>4</sup>The plateau at  $F_1 \approx 2/3$  for  $\tau \rightarrow 0$ : At very small  $\tau$  the recovered  $\hat{B}$  is near-fully dense, so the predictor effectively guesses every directed cluster-pair as an edge: recall is 1 and precision is the fraction of cluster-pairs that are truly connected, which for  $\lambda = 0.5$  inter-block density gives precision  $\approx 1/2$  and hence  $F_1 \approx 2/3$ . The plateau at 1 for moderate  $\tau$  is the regime of true recovery.